Springer

KSME

Journal of Mechanical Science and Technology 24 (9) (2010) 1939~1946
www.springerlink.com/content/1738-494x
DOI 10.1007/s12206-010-0625-8

Conjugated heat transfer and temperature distributions in a gas turbine combustion liner under base-load operation †

Kyung Min Kim[1], Namgeon Yun[1], Yun Heung Jeon[1], Dong Hyun Lee[1], Hyung Hee Cho[1,*] and Sin-Ho Kang[2]

[1]*Department of Mechanical Engineering, Yonsei University, Seoul, 120-749, Korea*
[2]*Gas Turbine Technology Service Center, Korea Plant Service & Engineering (KPS), Incheon, 404-170, Korea*

(Manuscript received December 7, 2009; revised May 15, 2010; accepted June 4, 2010)

Abstract

Prediction of temperature distributions on hot components is important in development of a gas turbine combustion liner. The present study investigated conjugated heat transfer to obtain temperature distributions in a combustion liner with six combustion nozzles. 3D-numerical simulations using FVM commercial codes, Fluent and CFX were performed to calculate combustion and heat transfer distributions. The temperature distributions in the combustor liner were calculated by conjugation of conduction and convection (heat transfer coefficients) obtained by combustion and cooling flow analysis. The wall temperature was the highest on the attachment points of the combustion gas from combustion nozzles, but the temperature gradient was high at the after shell section with low wall temperature.

Keywords: At Gas turbine combustion liner; Conjugated heat transfer; Internal cooling passage; Thermal analysis

1. Introduction

In modern gas turbine engines for land-based power generation, turbine inlet temperature (or firing temperature) has been increased steadily to improve gas turbine performance. Accordingly, new material, thermal barrier coating (TBC), and advanced combined cooling methods [1, 2] have been developed to improve reliability and durability of the hot components. Of late, NOx has been an environmental problem and it has attracted worldwide attention. High flame temperature of more than 2,000K in traditional gas turbine combustors with convectional combustion type results in relatively high NOx emissions. One approach to reducing NOx emissions has been to premix the maximum possible amount of compressor air with fuel. In an advanced combustor system for NOx reduction, the maximum possible amount of air is premixed with the fuel, so that flame temperatures and NOx of the premixed combustion emissions become lower than those of the convectional combustion. [3]

Many combustors in modern gas turbines have not applied film cooling for directly decreasing the flame temperature. In general, the combustion liner has been protected from hot combustion gas using forced convectional cooling methods such as jet impingement cooling and rib roughened surfaces. Therefore, wall temperature prediction by conjugated conduction and forced convection between hot gas and cooling air plays a key role in a combustor system design. Moreover, accurate prediction of conjugated heat transfer distributions on external and internal metal surfaces is also important in cooling system designs for new concept and modification. Recently, many researchers [4-7] have investigated methodologies and characteristics of the conjugated heat transfer including conduction and convection. Thus thermal analysis becomes an important issue in order to enhance the heat transfer as well as to reduce the thermal stress yielded by temperature gradients.

To calculate the wall temperature distributions, wall adjacent temperatures and wall heat transfer coefficients are required. It is difficult experimentally to obtain wall adjacent temperatures and wall heat transfer coefficients under high temperature and pressure environment, and complicated geometry. However, lately, computational fluid dynamics (CFD) codes have become a powerful design tool with developing of conjugated heat transfer solver, and turbulence models. Many researchers [8-15] have performed CFD prediction including combustion, fluid flow, and heat transfer in the gas turbine combustors. In addition, Tinga et al. [16] predicted lifecycle in a gas turbine blade and Yun et al. [17, 18] predicted lifetime in a gas turbine combustion liner using the material temperature and thermal stresses. Various technical papers or gas turbine

† This paper was recommended for publication in revised form by Associate Editor Man Yeong Ha

* Corresponding author. Tel.: +82 2 2123 2828, Fax: +82 2 312 2159
E-mail address: hhcho@yonsei.ac.kr

analysis have been published using numerical methods. However, the internal and external heat transfer data of the previous researcher are difficult to use in conjugated problems. It is because the heat transfer coefficients are affected by various design parameters, such as thermal wall boundary conditions, liner shapes, combustor nozzles, and so on.

In the present paper, conjugated heat transfer to obtain temperature distributions in a gas turbine combustion liner is calculated using CFD commercial codes, ANSYS Fluent and CFX for an actual combustor geometry. The objectives of the present investigation are (1) to obtain an accurate temperature distribution by solving conjugated heat transfer problems with an actual gas turbine operating condition; and (2) to obtain reliable temperature data in order to analyze deformation, thermal stresses, and lifetime. Further, the information on the heat transfer coefficients by hot gas and cooling air, the maximum temperature on metal and TBC, and the temperature gradient between the top and the bottom of each material can help many researchers to select super-alloy and thermal barrier coating (TBC) materials and to decide experimental conditions for improving capability of super-alloy and TBC.

2. Research methods

2.1 Configuration of the combustion liner

The present study was performed for conjugated thermal analysis of a gas turbine combustion liner with firing temperature of approximately 1600K in base-load operation. The combustion liner [19, 20] among its components is divided into three outside parts (forward shell section, center shell section, and after shell section) as shown in Fig. 1. Each section has different cooling methods. The forward shell, the center shell, and the after shell sections are cooled by rib-roughened passage, impingement jet, and C-channel, respectively. Among these sections, the after shell section is cooled using an internal passage cooling method because this section is inserted into a transition piece. It is called a C-channel, but the present study simplifies the after shell section ignoring the C-channel. Detailed analysis of this section was investigated in the previous study of Kim et al. [21].

The overall temperature distributions can be analyzed using the heat transfer coefficients and the wall adjacent temperature inside and outside the combustion liner. However, the combustion liner has very complex structures. Therefore, we calculated the wall adjacent temperature analysis for a part inside the combustion liner, and then conjugated heat transfer analysis of both the inside and the outside.

2.2 Modeling inside combustion liner

Fig. 2(a) shows the schematic for the analysis of the combustion field with six premixed nozzles, which are five identical outer burners and one smaller center nozzle. The combustion liner and 6 premixed nozzles are considered to calculate flow temperature and heat transfer distributions in the 3D

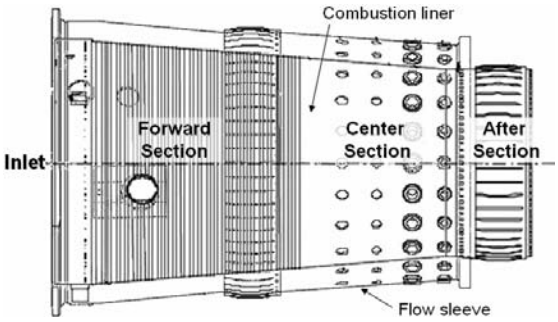

Fig. 1. Schematics of combustion liner and flow sleeve.

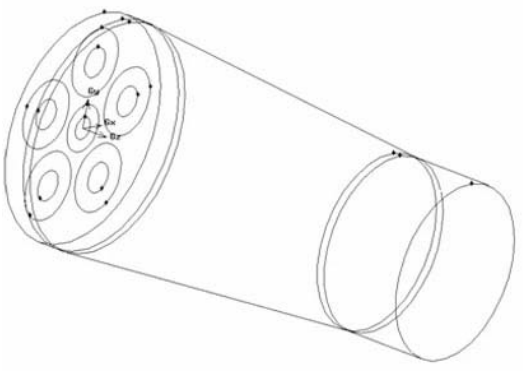

(a) Combustion flow space and fuel nozzles

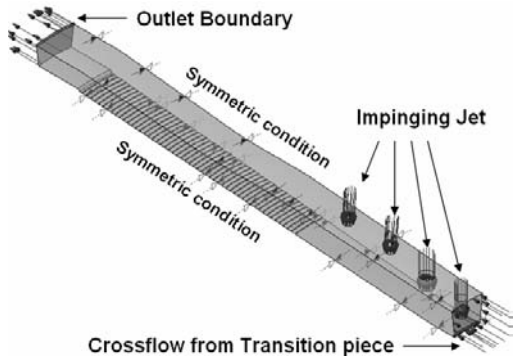

(b) Cooling flow space between combustion liner and flow sleeve

Fig. 2. Modeling for flow and heat transfer analysis.

combustion field using a commercial code, Fluent 6.3.

The domain in the combustion liner ranges from the assembly of nozzle cap to the combustion liner end (approximately 900 mm). The inner diameter of the nozzle cap is 457 mm and that of the combustion liner connecting with the transition piece is 349 mm. Structured grids are generated using GAMBIT and the grid consists of approximately 0.5 million cells with a minimum y^+ of about 1.0 from a grid independency test [22]. For the turbulence model and the wall function are selected k-ε model and enhanced wall function, respectively. The actual base-load operating condition is applied to combustion flow in the present analysis. The angle of swirl vanes located at the outlet of the nozzles is 50° and the after

section is treated as a simplified shape. As for the base-load operation condition, the fuel gas is assumed to be CH_4 occupying most of the natural gas, the mass flow rate of the fuel gas is 0.69 kg/s, the equivalence ratio is 0.38, average pressure in the combustion chamber is 15.2 atm and the fuel temperature at the inlet of the nozzles is 675.56K. The turbulence model is Realizable k-ε model and the combustion model is a partially premixed combustion model. The process of the combustion is considered as the following equation for reaction.

$$CH_4 + 2\,(O_2 + 3.76N_2) \rightarrow CO_2 + 2H_2O + 7.52N_2 \quad (1)$$

2.3 Modeling outside combustion liner

Fig. 2(b) shows the modeling outside the combustion liner coolant side for flow and heat transfer analysis by cooling air. To analyze the flow and heat transfer characteristics outside the objective combustion liner, 3-dimensional analysis was performed using commercial codes, GAMBIT and CFX-11. The forward section and the center section in the combustion liner are cooled by both rib-roughened surface on the combustion liner and impinging jet holes on the flow sleeve, respectively. The array of the cooling holes in the center section is twenty-four rows on the circumference of the flow sleeve, and each row is composed of four holes. The present analysis is performed for one twenty-fourth of the channel formed between the flow sleeve and the liner because the shape has a symmetric behavior. The mass flow rate of the coolant air per cooling hole is set at 0.1 kg/s. The crossflow rate from the transition piece is assumed at 1.7 kg/s, which is calculated from the flow rate impinged by transition piece cooling holes. The Reynolds number based on the hydraulic diameter of the channel is about at 550,000 in consideration of the operation data under the base load. Unstructured grids are generated using GAMBIT and the grid consists of approximately 1.15 million cells from a grid independency test. SST low Reynolds model is selected for the turbulence model [23].

2.4 Conjugated heat transfer analysis

As aforementioned, the overall temperature distributions are analyzed using the heat transfer coefficients and the wall adjacent temperature inside and outside the combustion liner. Thus, the present study is investigated, divided into inside and outside parts of the combustion liner. First, we calculate the wall adjacent temperature in the inside combustion part. Second, we calculate the heat transfer coefficients in the outside cooling part. Next, we calculate the heat transfer coefficients in the inside combustion part using the second step results, both the outside heat transfer coefficients and the bulk temperature of the coolant flow. Finally, we obtain temperature by conjugated heat transfer of conduction in metal and TBC of the combustion liner. The material properties of metal and TBC are based on Ninomic 263 [24] and yttria-stabilized zirconia (YSZ) coating. The thermal conductivities of metal and TBC are presented in Table 1.

Table 1. Thermal conductivities of metal and TBC as a function of temperature.

Temperature [°C]	Metal [W/m-°C]	TBC [W/m-°C]
100	13.0	-
200	14.7	-
400	18.0	2.1
600	21.4	2.13
800	24.7	2.2
1000	28.5	2.3
1100	-	2.35
1200	-	2.4

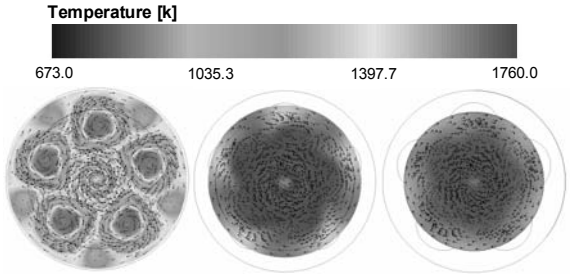

(a) Entrance (b) Center (c) Exit

Fig. 3. Flow and temperature distributions in cross sections.

3. Results and dscussion

3.1 Heat transfer inside the combustion liner

Figs. 3 and 4 show flow structures and temperature distributions by mixing hot combustion gas from six nozzles with coolant compressed air around the nozzles. Fig. 3 is the result at the three cross-sections (*y-z* plane), and Fig. 4 is the result at the horizontal plane to the axial direction (*x-y* plane). The six swirling flows are formed because of the nozzle guide vanes as shown in Fig. 3(a). The five swirls at the outer side of the cross section appear to form clockwise rotating flows as a view from the entrance of the combustion liner, but the one swirl at the center swirler appears to form counter-clockwise rotating flow. The temperature inside the nozzles is high due to combustion. As the flow passes along the combustion liner, the six swirling flows are changed to two large swirling flows, outer clockwise rotating flow and inner counter-clockwise rotating flow as a view from the entrance of the combustion liner. As presented in Figs. 3(b) and 3(c), the rotating flow disappears in the flow region between inner and outer sides since the two large swirling flows intersect each other. Therefore, the flow with high velocity and high temperature goes through this intersection region, so that the temperature and flow velocity become high. That is, the temperature and velocity in the outer and inner sides are lower than those in the intersection region as shown in Fig. 4. In the outlet of combustion liner, the averaged temperature is approximately 1740K.

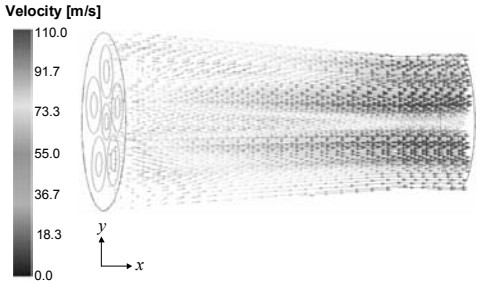

(a) Velocity vectors

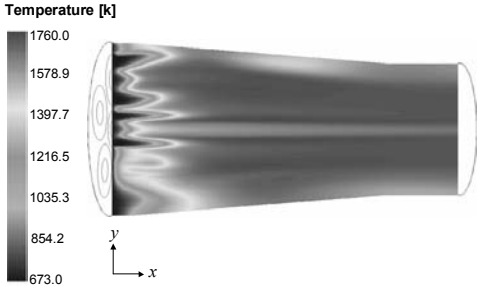

(b) Temperature contours

Fig. 4. Velocities and temperature distributions by combustion.

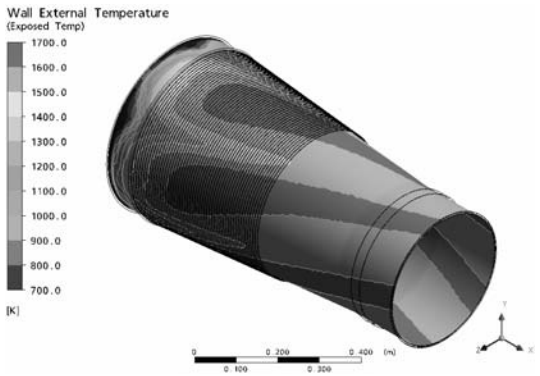

(a) Contour plot

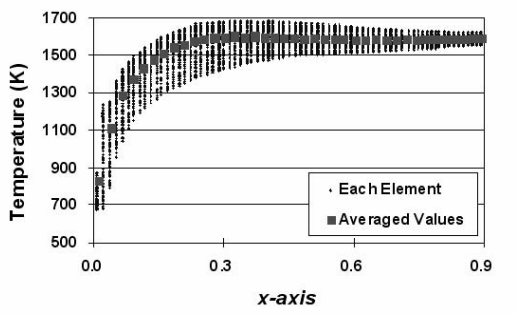

(b) Local values on elements

Fig. 5. Distributions of wall adjacent flow temperature.

Fig. 5 presents wall adjacent temperature distributions on the combustion liner in contour 5(a) and local 5(b) plots. The temperature results from mixing and conduction between the cooling air and the hot gas. The high temperature distributions are changed to clockwise direction by swirling flow as shown in Fig. 3(a). Since the swirls of the combustion gas along the combustion liner are weakened gradually, the temperature

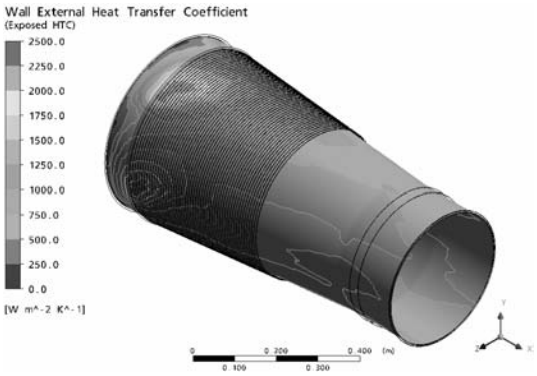

(a) Contour plot

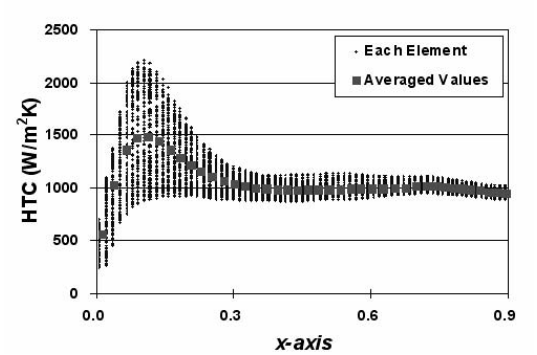

(b) Local values on elements

Fig. 6. Distributions of heat transfer coefficients by combustion.

difference between the maximum and the minimum values in flow direction becomes narrow as shown in Fig. 5(b). In addition, the circumferential-averaged temperature value becomes uniform after approximately 0.3 m from the inlet of the combustion liner as shown in Fig. 5(b). The circumferential-averaged temperature is approximately 1,540K at the end. It is noted that the maximum temperature is lower, but the minimum temperature is higher than those at the location of approximately 0.3 m.

Fig. 6 shows the wall heat transfer coefficient distributions inside the combustion liner induced by the swirling flows of combustion gas. The wall heat transfer coefficients in circumferential direction are varied largely at the forward section of the combustion liner like the wall adjacent temperature distribution. The values at 0.12 m from the liner inlet range from 850 W/m^{2}K to 2,200 W/m^{2}K. The region with high value and wide range is located in front of the point with the high wall adjacent temperature. It is noted that the mixing between hot gas and cooling air is active in this location; moreover, the combustion gas is attached in this region which is located at approximately 0.1 m from the liner inlet. After 0.3 m from the liner inlet, the heat transfer coefficients approach gradually a constant value (about 1,000 W/m^{2}K) near the after section.

3.2 Heat transfer outside the combustion liner

Fig. 7 shows the heat transfer distributions outside the combustion liner coolant side. In contour 7(a) and local 7(b) plots the overall heat transfer coefficients have symmetric behavior

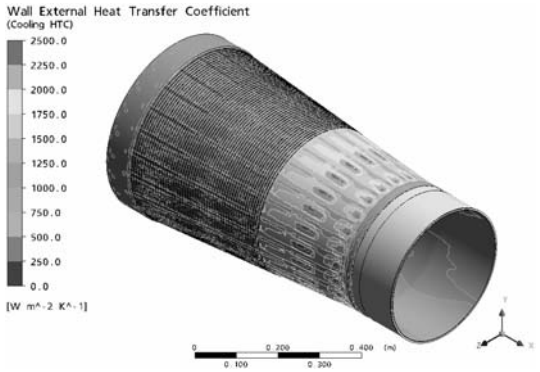

(a) Contour plot

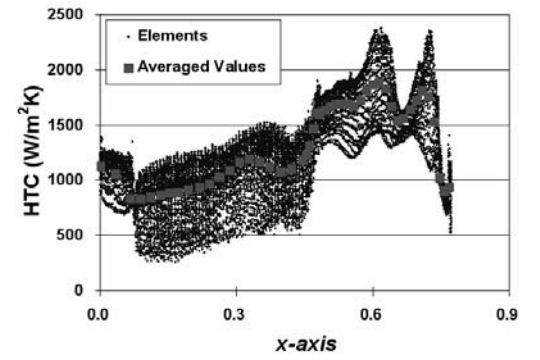

(b) Local values on elements

Fig. 7. Distributions of heat transfer coefficients by cooling flow.

because cooling holes are regularly arranged. By the impinging jets of the coolant air, high heat transfer appears on the outside surface of the combustion liner. The heat transfer coefficients induced by the first and the second cooling holes from the liner exit are approximately 2,300W/m^{2}K. The high heat transfer region is moved toward the forward section rather than location below the cooling holes. The reason is that the impinging flows are deflected by the effect of the cross flow from the transition piece backward flow. Heat transfer enhancement by the impinging coolant air of the third and fourth holes is smaller than that by the first and the second holes due to the cross flow. The values are approximately 1,800 and 1,500 W/m^{2}K, respectively.

After the impinged cooling flow is added to the crossflow from the transient piece, the accumulated flow toward the forward section and the rib tabulators formed on the surface outside the liner enhance the heat transfer. The enhanced values range from 800 to 1,000 W/m^{2}K. As the coolant flow goes toward the liner entrance, the heat transfer coefficients decrease. It is because the cooling passage becomes larger with the diameter of combustion liner.

3.3 Temperature distributions in the combustion liner

Fig. 8 shows the wall temperature distributions on three surfaces, such as TBC surface (hot gas side), interface, and metal surface (cooling side). Fig. 9 presents the local wall temperature distributions TBC material and metal material and the

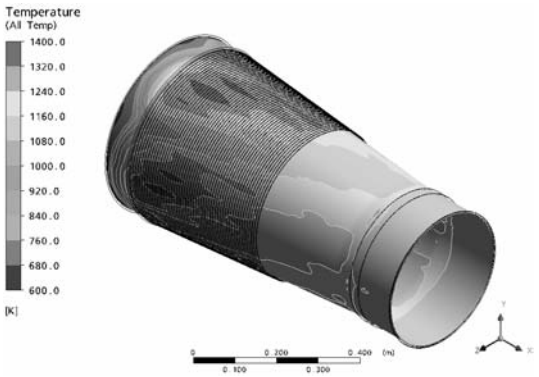

(a) TBC surface (hot gas side)

(b) Interface between metal and TBC

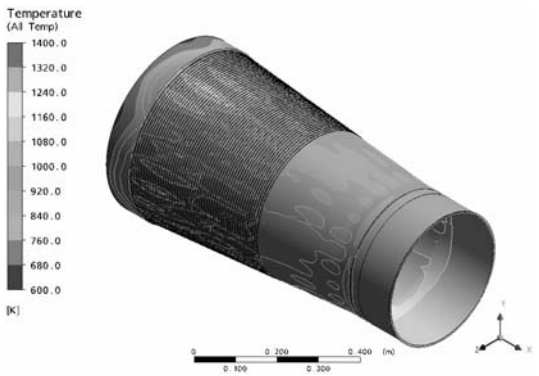

(c) Metal surface (cooling side)

Fig. 8. Contour plots of wall temperature distributions.

maximum and minimum temperature on all three surfaces. As shown in Fig. 8, the overall patterns of temperature distributions are similar to the pattern of wall adjacent temperature (Fig. 5(a)). However, the temperature distributions on the metal surface of cooling side are more uniform than those on the TBC surface. The maximum temperature in TBC material is about 1270K at 0.17 m of *x*-axis as shown in Fig. 9(a). This location is the same to the attachment points of the combustion gas from combustion nozzles. At this location, the difference in temperature among circumferential distributions is the largest, such as approximately 360K. This temperature difference can cause high thermal stress. After this location with the highest temperature, the high temperature becomes lower and the difference becomes smaller, because the high heat transfer

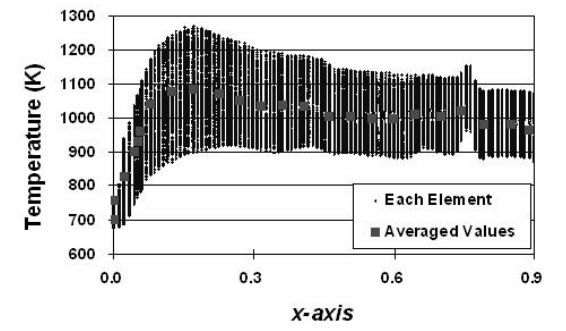

(a) TBC material (hot gas side)

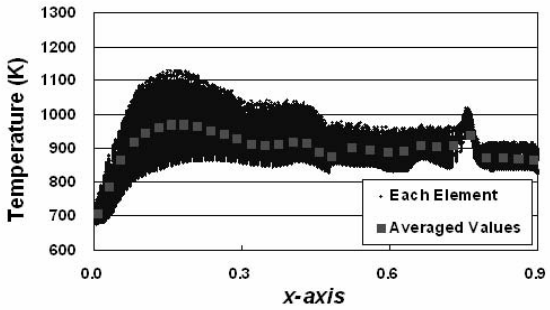

(b) Metal material (cooling side)

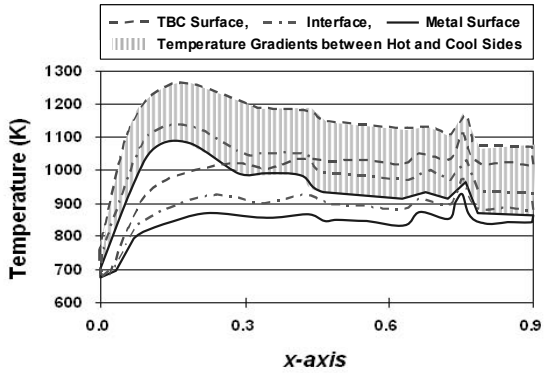

(c) Each surface

Fig. 9. Local wall temperature distributions.

coefficients are induced by impingement jet cooling in the center section of the combustion liner. The characteristics of temperature in metal material (Fig. 9(b)) are similar to those in TBC material. The maximum temperature on metal material is 1,130K at 0.14 m of *x*-axis. The largest temperature difference among circumferential distributions is approximately 280K. At the exit of the liner, the temperature difference is smaller than 100K. The reason is that the thermal conductivity of the metal is high and the applied cooling is effective.

Fig. 9(c) shows the maximum and minimum wall temperature distributions on each surface (TBC surface, interface, and metal surface). Temperature gradients between the hot gas side and the cooling side at the highest temperature in circumferential direction can be also analogized from this Fig. as symbolized by gray columns. These temperature gradients are induced by the conjugation of thermal conductivities of TBC and metal, the gas temperatures, and the heat transfer coefficients of hot and cooling sides. The temperature gradients are large at the after shell section of the low wall temperature, but small at toward the section of the high wall temperature. It is noted that a high temperature gradient induces high thermal stress, resulting in thermal creep. This is why the after shell section is damaged often even though the wall temperature is lower than the forward section.

4. Conclusions

The present paper investigated conjugated heat transfer and temperature distributions in a gas turbine combustion liner in order to predict the weak points of hot components and support the test conditions in design of a combustion liner. The material temperature greatly depends on the heat transfer coefficients on external and internal liner surface. The main conclusions are summarized as follows:

(1) In the pre-mixed combustion liner, the mixing between the hot gas and the coolant air is active before 0.3 m from the liner inlet, so that the heat transfer coefficients increase sharply in the forward section. After 0.3 m, the heat transfer coefficients and the temperature approach plateau values, which are approximately 1,000 W/m^{2}K and 1,540K, respectively.

(2) The heat transfer coefficients range from 800 to1,000 W/m^{2}K on the rib-roughened surface in the forward section. The heat transfer coefficients are enhanced to 2,400 W/m2K on the surface impinged by the first and the second holes of the center section. However, the high heat transfer region is deflected toward the forward section by crossflow from the transient piece.

(3) The overall temperature distributions are similar to the wall adjacent temperature. The maximum temperatures in TBC and metal materials are about 1,270K and 1,130K, respectively. The temperature gradients are high at the after shell section low wall temperature, but low at the forward section of high wall temperature.

Acknowledgment

This work was supported by the Power Generation & Electricity Delivery of the Korea Institute of Energy Technology Evaluation and Planning (KETEP) grant funded by the Korea government Ministry of Knowledge Economy.

References

[1] B. Weigand and S. Spring, Multiple jet impingement – A review, Int. Symp. on Heat Transfer in Gas Turbine Systems, Antalya, Turkey (2009).

[2] K. H. Park, K. M. Yang, K. W. Lee, H. H. Cho, H. C. Ham and K. Y. Hwang, Effects of injection type on slot film cooling for a ramjet combustor, Journal of Mechanical Science and Technology, 23 (2009) 1852-1857.

[3] E. Divo, E. Steinthorsson, F. Rodriguez, A. J. Kassab and J.

S. Kapat, Glenn-HT/BEM conjugate heat transfer solver for large-scale turbomachinery models (2003) NASA-Report CR 212195.

[4] K. M. Kim, D. H. Lee, H. H. Cho and M. Y. Kim, Thermal analysis of a film cooling system with normal injection holes using experimental data, Int. J. of Fluid Machinery and Systems, 2 (2009) 55-60.

[5] M. Kane and S. Yavuzkurt, Calculation of gas turbine blade temperatures using an iterative conjugate heat transfer approach, Int. Symp. on Heat Transfer in Gas Turbine Systems, Antalya, Turkey (2009).

[6] S. Siw, M. K. Chyu, W. Slaughter, V. Karaivanov and M.A. Alvin, Influence of internal cooling configuration on metal temperature distributions of future coal-fuel based turbine airfoils, ASME Turbo Expo 2009, Orlando, FL, USA (2009) GT2009-59829.

[7] H. Lefebvre, Gas turbine combustion, 2nd ED., Taylor and Francis, Philadelphia (1999).

[8] S. Choi, D. Lee and J. Park, Ignition and combustion characteristics of the gas turbine slinger combustor, Journal of Mechanical Science and Technology, 22 (2008) 538-544.

[9] A.D. Gosman and E. Ioannides, Aspects of computer simulation of liquid-fueled combustors, Journal of Energy, 7 (6) (1983) 482-490.

[10] D. S. Fuller and C. E. Smith, Integrated CFD modeling of gas turbine combustors, AIAA 29thJoint Propulsion Conference and Exhibit, Monterey, CA, USA (1993) AIAA-1993-2196.

[11] E. J. Fuiler and C. E. Smith, CFD analysis of a research gas turbine combustor primary zone, 30th Joint Propulsion conference, Indianapolis (1994) AIAA-94-3271.

[12] D. Giebert, E. Papanicolaou, C.-H. Rexroth, M. Scheuerlen, A. Schulz and R. Koch, Numerical Modelling of Combustor Liner Heat Transfer, High Intensity Combustions - Steady Isobaric Combustion (2002) 282-298.

[13] J. C. Bailey, J. Intile, T. F. Fric, A. K. Tolpadi, N. V. Nirmalan and R. S. Bunker, Experimental and numerical study of heat transfer in a gas turbine combustor liner, ASME Journal of engineering for gas turbines and power, 125 (4) (2003) 994-1002.

[14] O. Liedtke and A. Schulz, Development of a new lean burning combustor with fuel film evaporation for a micro gas turbine, Experimental Thermal and Fluid Science, 27 (4) (2003) 363-369.

[15] S. P. Woo and I.-S. Jeung, A study on the flow characteristics of gas turbine engine combustor on/off the operation envelope, 5th Asia-Pacific Conference on Combustion, The University of Adelaide, Australia (2005) 161-164.

[16] T. Tinga, J. F. Kampen, B. D. Jager and J. B. W. Kok, Gas turbine combustion liner life assessment using a combined fluid/structural approach, ASME J. of Engineering for Gas Turbines and Power, 129 (2007) 69-79.

[17] N. Yun, Y. H. Jeon, K. M. Kim, D. H. Lee and H. H. Cho, Thermal and creep analysis in a gas turbine combustion liner, the 4th IASME/WSEAS International Conference on Energy & Environment, University of Cambridge, UK (2009).

[18] N. Yun, K. M. Kim, Y. H. Jeon, D. H. Lee, H. H Cho and M. Y. Kim, Thermal characteristics in a gas turbine combustion liner with firing temperature of 1600K, KSME 2008 Fall Annual Meeting (2008) 2984-2988. (In Korean).

[19] V. C. Martling and Z. Xiao, Combustion liner having improved cooling and sealing, United States Patent, (2007) No. US7269957 B2.

[20] J. C. Intile, J. A. West and W. Byrne, Method and apparatus for cooling combustion liner and transition piece of a gas turbine, United States Patent (2007) No. US7010921 B2.

[21] K. M. Kim, N. Yun, Y. H. Jeon, D. H. Lee and H. H. Cho, Failure analysis in after shell section of gas turbine combustion liner under base-load operation, Engineering Failure Analysis (2009) Under Review.

[22] ANSYS FLUENT, FLUENT 6.3 User's Guide, Fluent Inc., Lebanon, USA (2006).

[23] ANSYS CFX, ANSYS CFX User's Guide, Release 11.0, ANSYS Inc., Canonsburg, USA (2007).

[24] Special Metals. Product handbook of high-performance alloys. Special Metals Corporation 2007; Publication No. SMC-054.

Kyung Min Kim received his PhD in Mechanical Engineering from Yonsei University, Seoul, Korea in 2008. He is currently a research professor in Yonsei University.

Namgeon Yun received his M.S. in Mechanical Engineering from Yonsei University, Seoul, Korea in 2009. In 2009, he joined the Doosan heavy industries & Construction Co, Ltd, where he is a member of the IGCC Team.

Yun Heung Jun received his PhD in Mechanical Engineering from Yonsei University, Seoul, Korea in 2009. In 2001, he joined Korea Western Power Co, Ltd, where he is currently working as a section chief.

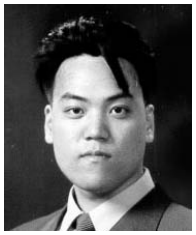

Dong Hyun Lee received his PhD in Mechanical Engineering from Yonsei University, Seoul, Korea in 2009. He is currently a Post-Doc Fellow in Yonsei University.

Hyung Hee Cho received his PhD in Mechanical Engineering from University of Minnesota, Minneapolis, MN in 1992. In 1995, he joined the Department of Mechanical Engineering, Yonsei University, Seoul, Korea, where he is currently a full professor in the School of Mechanical Engineering.

Sin-Ho Kang received his PhD in Mechanical Engineering from Yonsei University, Seoul, Korea in 2006. In 1993, he joined Korea Plant Service & Engineering (KPS), Incheon, Korea, where he is currently a Principal Researcher.